Static and dynamic properties of the classical XY chain in a transverse magnetic field

R. W. Gerling* and D. P. Landau
Center for Simulational Physics, University of Georgia, Athens, Georgia 30602
(Received 19 May 1987)

We present extensive computer-simulation results for the static and dynamic properties of the one-dimensional classical XY model in a symmetry-breaking magnetic field. In-plane solitons are directly observed and their density is determined as a function of field and temperature. The bulk properties and the scattering function $S(q,\omega)$ are also determined, but while they show spin-wave contributions they do not provide any clear evidence of soliton behavior. Our simulation results are compared with theoretical predictions.

I. INTRODUCTION

One-dimensional planar magnets have been studied intensely over the last few years.[1-10] These magnets are systems whose static and dynamic properties are believed to exhibit soliton or solitonlike features, if one direction in the plane is made preferable. (In general, references to these systems do no use the word "soliton" in the strict mathematical sense but rather to imply kinklike behavior.) The system most studied theoretically is the one-dimensional classical Heisenberg model with easy-plane anisotropy;[1-5] and experimentally it is $CsNiF_3$.[6-9] The different studies carried out in this field were reported in 1984.[10] Despite extensive recent activity, the field is still the subject of some controversy.

Mikeska showed[1] that, using certain approximations, the isotropic Heisenberg chain with single-ion (easy-plane) anisotropy can be mapped onto the sine-Gordon model, the thermodynamics of which have been discussed by several authors.[11,12] This mapping provides a description of time-dependent behavior and a simple picture has been developed in which the solitons are regarded as quasiparticles with finite mass and thermal distribution of velocities. In ferromagnetic chains, solitons correspond to moving domain walls, separating regions with a spin-phase difference of 2π. Neutron scattering,[6,7] specific-heat,[9] and spin-lattice relaxation-time[8] measurements claim evidence for spin solitons in $CsNiF_3$, although some authors question this interpretation.[13] The importance of the quantum-mechanical nature of $CsNiF_3$ with regard to soliton behavior is still unclear (see e.g., in Ref. 10). In order to eliminate any uncertainty about the role of quantum effects, we wish to study a purely classical system for which we can carry out a computer simulation as an ideal classical experiment. We choose for our computer simulation the simplest model which can be mapped onto the sine-Gordon model: the classical XY chain in a magnetic field. The Hamiltonian is given by

$$\mathcal{H}=-J\sum_{(i,j)}(S_i^xS_j^x+S_i^yS_j^y)-h\sum_i S_i^x\ , \tag{1}$$

where the sum (i,j) runs over all nearest-neighbor pairs and the $\mathbf{S}_i$ are three-dimensional classical vectors of unit length. J is the exchange-coupling constant and $h=g\mu_BH$ a magnetic field in the x direction. The exchange anisotropy makes it energetically favorable for the spins to lie in the XY plane. The field tends to align the spins parallel to the positive x axis. Our results can then be used to determine the suitability of the sine-Gordon mapping, or other theories, for a purely classical model.

We have used a standard Monte Carlo method together with a spin dynamics approach to study the model system. Details of these methods are described in Sec. II of this paper. The results are presented in Sec. III including both static and dynamic behavior. In Sec. IV, we summarize and draw conclusions.

II. METHOD

Equilibrium spin configurations were generated using a single "spin-flip" importance-sampling Monte Carlo method.[14] We used an algorithm which reoriented single spins by comparing a random number to the exponential of the energy change. By dividing the chains into two sublattices (even and odd spins) we could vectorize the algorithm on the Cray Research X-MP Computer and on the Control Data Corporation Cyber 205 computer. We typically took spin chains with $N=2000$ spins and periodic boundary conditions. As described earlier[15] we performed 1500 Monte Carlo steps (MCS's) per spin at each temperature and magnetic field value. The first 500 MCS's per spin were not retained, allowing the system to reach equilibrium. At some values of temperature and field many more MCS's were necessary, and we retained between 5×10^3 and 3×10^4 MCS's/site for computing averages after first discarding between 5×10^3 and 2×10^4 MCS's/site, respectively. For each data set, such a Monte Carlo run was repeated six times and the results averaged. Even with these statistics the error in the specific heat was as large as 10% for some range of temperature and field. This surprising result agrees with the findings of other authors[16] for an easy-plane chain. Data were obtained on the Cyber 205 at the University of Georgia. (Some of the early Monte Carlo data were obtained using the Cray X-MP at the Kernforschungsanlage Jülich.)

The specific heat was calculated both by numerically

differentiating the internal energy and from the fluctuations of the energy. Normally both methods give the same result. For temperatures smaller than 0.4 J we had difficulties reaching equilibrium, which was indicated by the fact that the two methods could give slightly different answers.

We have calculated the in-plane angle φ_i of each spin with respect to the x axis. By taking the angle between two nearest-neighbor spins $\Delta\varphi_i=\varphi_i-\varphi_{i-1}$, we obtain the phase of the nth spin from the sum

$$\phi_n=\varphi_1+\sum_{i=2}^{n}\Delta\varphi_i \ . \tag{2}$$

The spin phase angle ϕ_n in the XY plane versus position is plotted for states separated by 200 MCS's per spin to ensure that the phase angle plots are statistically independent. A soliton can be seen easily as a phase jump of 2π in these plots.

Specially selected spin states containing one or two solitons are used as starting configurations for a spin dynamics simulation, which is used to study the time development of the solitons.

The equation of motion for the XY model is

$$\frac{\partial}{\partial t}\mathbf{S}_i=\mathbf{S}_i\times[J(S_{i-1}^x+S_{i+1}^x)\hat{\mathbf{e}}_x +J(S_{i-1}^y+S_{i+1}^y)\hat{\mathbf{e}}_y+h\hat{\mathbf{e}}_x] \ , \tag{3}$$

where $\hat{\mathbf{e}}_x$, $\hat{\mathbf{e}}_y$, and $\hat{\mathbf{e}}_z$ are the unit vectors in the x, y, and z directions. Equation (3) can be obtained as canonical equations of motion corresponding to the Hamiltonian (1) as

$$\dot{\varphi}_i=\frac{1}{JS^2}\frac{\partial\mathcal{H}}{\partial(\sin\theta_i)} \ , \tag{4a}$$

$$\frac{d}{dt}(\sin\theta_i)=-\frac{1}{JS^2}\frac{\partial\mathcal{H}}{\partial\varphi_i} \ . \tag{4b}$$

where the angles φ_i play the role of generalized coordinates and the z components $[\sin(\theta_i)]$ of the spin vectors play the role of the corresponding canonical momenta.[17]

The integration of Eq. (3) was performed by using the formula[18]

$$\mathbf{S}_i(t+\Delta)=\mathbf{S}_i(t-\Delta)+2\dot{\mathbf{S}}_i(t)\Delta+\tfrac{1}{3}\ddot{\mathbf{S}}_i(t)\Delta^3+O(\Delta^5) \ , \tag{5}$$

where Δ is the time increment of the integration. To obtain $\ddot{\mathbf{S}}_i$ we must differentiate Eq. (3) twice with respect to time. After several time steps, we again plotted the phase ϕ_n of the spins to see the time development of the solitons. We typically used an integration interval $\Delta=0.005/J$, resulting in a maximum useful integration time of $t=30/J$. Carrying out the time integration with different time increments and looking at the constants of motion, one can test the accuracy of the integration routine. The constants of motion are not the only way to test the quality of our integration. Correlation functions which have to be positive by definition (e.g., time-dependent energy-energy correlation function) indicate problems with the accuracy of the time integration by becoming negative. Our tests have shown[15] that the integration routine works extremely well.

We usually performed five spin dynamics runs using different initial states for the same temperature and field. The results we present are averages over these runs. From each of the five time integrations, time-displaced correlation functions are extracted:

$$\langle E_i(0)E_i(t)\rangle=\frac{J^2}{N}\sum_i[S_i^x(0)S_{i+1}^x(0)+S_i^y(0)S_{i+1}^y(0)+h/JS_i^x(0)][S_i^x(t)S_{i+1}^x(t)+S_i^y(t)S_{i+1}^y(t)+h/JS_i^x(t)] \ , \tag{6a}$$

$$\langle\mathbf{S}_i(0)\mathbf{S}_{i+r}(t)\rangle_\perp=\frac{1}{N}\sum_i[S_i^x(0)S_{i+r}^x(t)+S_i^y(0)S_{i+r}^y(t)] \ , \tag{6b}$$

$$\langle\mathbf{S}_i(0)\mathbf{S}_{i+r}(t)\rangle_\parallel=\frac{1}{N}\sum_i S_i^z(0)S_{i+r}^z(t) \ . \tag{6c}$$

These are averaged over the different runs and the last step in the computer program performs a double Fourier transform of the spin-spin correlation functions to yield the scattering function $S(q,\omega)$. To reduce cutoff effects, we introduced Gaussian spatial and temporal resolution functions.[19] We first performed the space Fourier transform by

$$\langle S(-q,0)S(q,t)\rangle_k=\sum_r^{r_{\max}}\cos(qr)\langle\mathbf{S}_i(0)\mathbf{S}_{i+r}(t)\rangle_k\exp[-\tfrac{1}{2}(r\,\Delta r)^2] \ . \tag{7}$$

The index k denotes the components parallel and perpendicular to the symmetry axis. The sum over r runs typically over 100 neighbors. The cutoff parameter Δr was chosen carefully to avoid spurious wiggles due to taking the Fourier transform of a function with a step, but at the same time avoiding excessive broadening. We obtained best results with $\Delta r=0.03$. After this we determined the time Fourier transform by

$$S_k(q,\omega)=\int_0^{t_{\max}}\cos(\omega t)\langle\mathbf{S}(-q,0)\mathbf{S}(q,t)\rangle_k\times\exp[-\tfrac{1}{2}(t\,\Delta t)^2]dt \ . \tag{8}$$

This integration was performed numerically and the time cutoff parameter Δt was chosen differently to find the best value. If Δt is too small we get large oscillations in the scattering function, if it is too large all structure is smeared out. We obtained best results with $\Delta t = 0.1 J^{-1}$. The dispersion curves can be determined from the positions of the spin-wave peaks.

III. RESULTS

A. Static properties

Figure 1 shows the internal energy as a function of temperature for different fields. The dependence on both is monotonic and nonsingular. For nonzero field the lines are a guide to the eye only, but for zero field the line is an analytic transfer integral result by Joyce.[20]

Currie, Krumhansl, Bishop, and Trullinger (CKBT) have developed the statistical mechanics of the sine-Gordon model.[11,21] They found a non-negligible contribution of the solitons to the free energy. This leads to a soliton induced peak in the magnetic field dependence of the specific heat. CKBT gave the result for the specific heat

$$c = c_H(T) - c_{H=0}(T) = k_B \left[\left[\frac{E_k^{(0)}}{k_B T} - \frac{1}{2} \right]^2 - \frac{1}{2} \right] n_k^{\text{tot}} , \tag{9}$$

where the soliton rest energy is $E_k^{(0)}$ and the soliton density is

$$n_k^{\text{tot}} = (8/\pi)^{1/2} \frac{1}{d} \left[\frac{E_k^{(0)}}{k_B T} \right]^{1/2} \exp \left[- \frac{E_k^{(0)}}{k_B T} \right] \tag{10}$$

and d is the soliton width. Equations (9) and (10) are results for the sine-Gordon model. In a continuum approximation we can express $E_k^{(0)}$ and d by the parameters of the Hamiltonian (1):[22]

$$E_k^{(0)} = 8(Jh)^{1/2} , \tag{11a}$$

$$d = (J/h)^{1/2} . \tag{11b}$$

Here we have already used the fact that the spins $\mathbf{S}_i$ have unit length and we measure all lengths in units of the nearest-neighbor spin distance.

Figure 2 shows the specific heat as a function of magnetic field for different temperatures. The specific heat predicted by Eq. (9) shows a maximum as a function of field at a fixed temperature. The positions of these peaks are indicated by arrows. The height of the peak is 0.1 for $k_B T = 0.15J$ and it increases to 0.3 for $k_B T = 0.45J$; thus soliton peaks should be seen clearly in Fig. 2. In contrast, the data show no indication of solitons whatsoever. The large peak which develops with increasing temperature is due to the uniform precession mode of the spins. At each data point, the Monte Carlo results are produced by making six different runs with 50 000 MCS's per spin each. For each run, 20 000 MCS's were not retained, allowing the system to equilibrate, and the specific heat was then calculated from the remaining 30 000 MCS's. The error bars were determined by treating these results as independent data and averaging over these six runs.

We also have calculated specific-heat data over a wider range of parameters (the data themselves are shown in Ref. 23) and from these data we have extracted the peak field for different temperatures. The maximum of the specific heat corresponds to the inflection points of the energy curves in Fig. 1. These results are plotted in a field-temperature plane in Fig. 3. The solid line is the

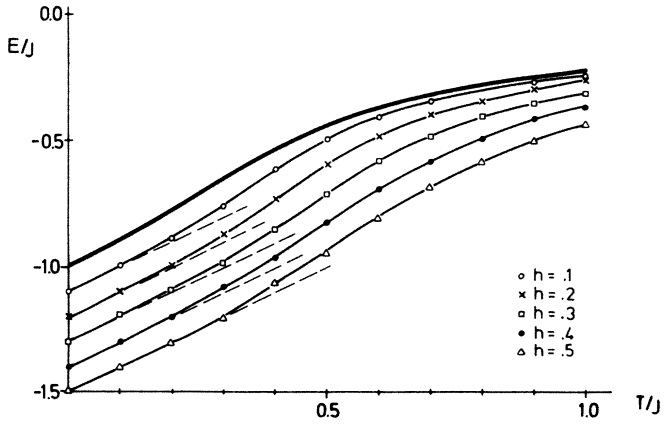

FIG. 1. The temperature dependence of the internal energy for different magnetic fields. The heavy solid line is the exact result of Joyce (Ref. 20) and the light solid lines are guides for the eye. The dashed lines indicate the initial slope where the internal energy is proportional to the temperature. The error is smaller than the size of the symbols.

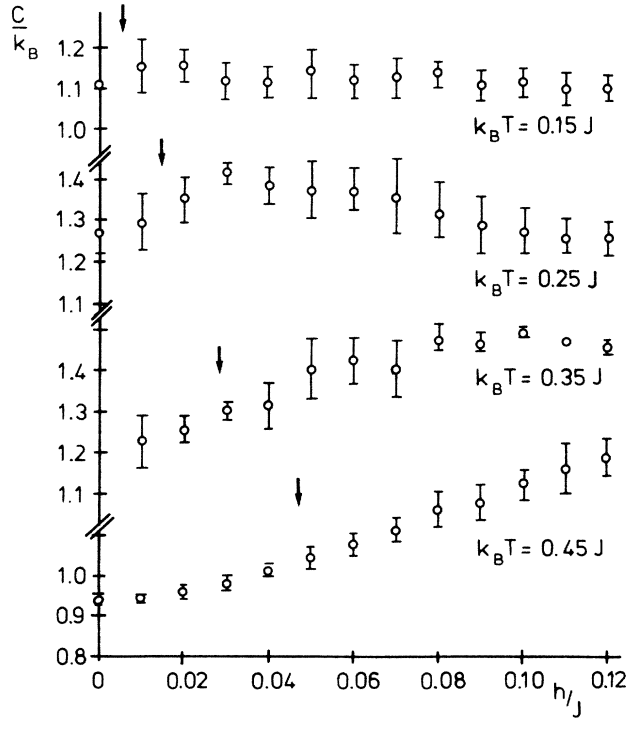

FIG. 2. Specific heat as a function of the field for different temperatures as indicated. The error bars are calculated from six different Monte Carlo runs. The arrows indicate the predicted positions of soliton-induced peaks.

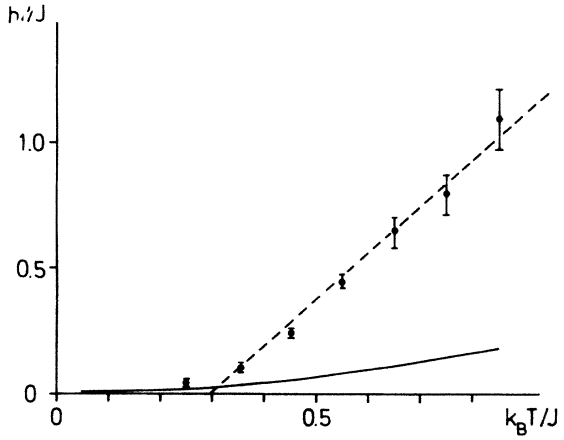

FIG. 3. The positions of the peaks in the specific heat in a temperature-field plane. The dashed line is a guide to the eye only and the solid line is the prediction by the sine-Gordon theory. Note the point at $k_BT=0.25J$.

sine-Gordon prediction (quadratic temperature dependence) and the dashed line is a guide for the eye only. The point for the lowest temperature ($k_BT=0.25J$) clearly deviates from the straight line, but this single point is not sufficient evidence for the presence of the sine-Gordon peak in the specific heat.

Figure 4 shows the x and y components of the static spin-spin correlation function as a function of distance for different fields. The y components decay exponentially to zero and the x components decay exponentially to a constant value which is the square of the magnetization. The z components are not plotted, because they are zero; there is no correlation between the z components of the spins. In Fig. 5, we show the temperature and field dependence of the inverse correlation length. The correlation length was calculated by fitting an exponential decay to the correlation functions. In the case of the x components the constant (square of the magnetization) was subtracted first.

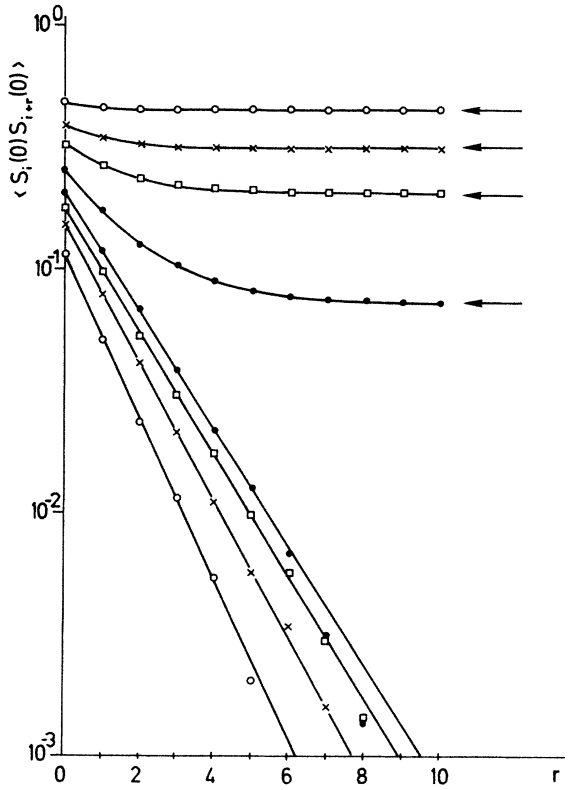

FIG. 4. Spin-spin correlation function of the x components (upper curves) and the y components (lower curves) as a function of distance r for different fields as indicated. The arrows indicate the corresponding value for $r=\infty$, which is the square of the magnetization.

Although the bulk properties give no clear indication of soliton contributions we were able to observe the solitons directly. In Fig. 6(a), a typical spin-phase plot is shown for a chain of 2000 spins. One soliton can be identified clearly as a phase jump of 2π. (The resolution is not good enough to see single spins.) Figure 7 shows a part of a spin chain on an enlarged scale so that single spins can be seen. Note that the temperature and field are different in Figs. 6 and 7. It is simple to measure the width of the solitons in Figs. 6 and 7. In Fig. 8 we show the soliton width as a function of inverse field. The soliton width was determined by fitting the shape function $\tanh(x)$ to the data points in Figs. 6 and 7. There is a good agreement between the Monte Carlo results and the sine-Gordon soliton width.

In Fig. 9 results for the density of solitons are given. The scales are chosen so that if sine-Gordon theory holds, all points should be on one line (the dashed line in Fig. 9). Our results show that the slope is reproduced properly (the slope corresponds to the soliton energy), but not the absolute value of the density. This result is in agreement with calculations by Jensen and Fogedby[24] who took the out-of-plane fluctuations of the spins into

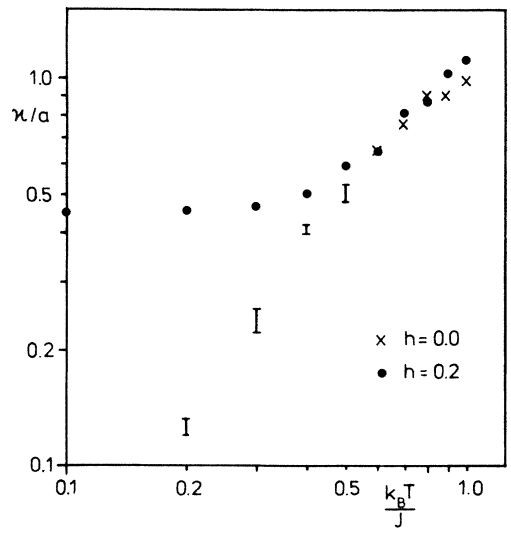

FIG. 5. The inverse correlation length as a function of temperature for different fields as indicated. The data were obtained by fitting an exponential decay to the spin-spin correlation functions. A constant due to a finite magnetiziation was subtracted first.

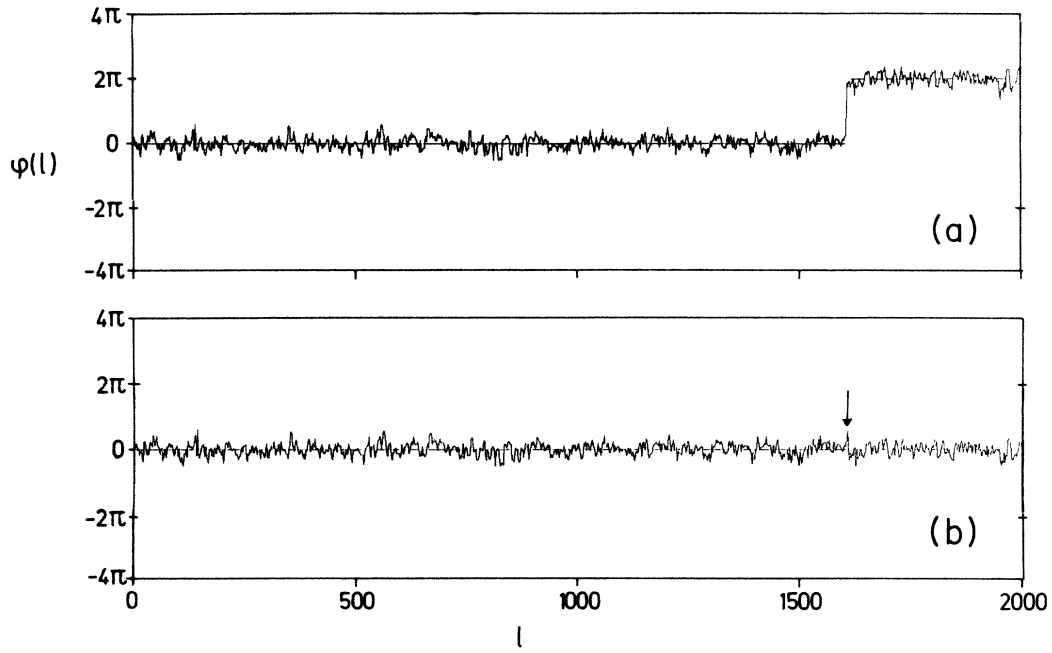

FIG. 6. A spin-phase plot for an entire chain of 2000 spins. $T=0.2J/k_B$ and $h=0.3J$. (a) This is a configuration containing one soliton which is used as a starting configuration for a spin dynamics run. (b) This is the result of the spin dynamics run after *only two* time steps of the integration (i.e., $t=0.01/J$): the soliton has disappeared. The arrow marks its former position. The field is above the stability field h_s.

account and found an enhancement of the soliton density. Looking at the solid lines in Fig. 9 we see that the enhancement factor depends linearly on the magnetic field. This also means that the soliton density approaches the sine-Gordon result (dashed line) as the field approaches zero. Of course, the sine-Gordon picture does not make any sense for zero field. The agreement between our Monte Carlo results and Jensen and Fogedby's calculation is qualitative but not quantitative.

B. Dynamic properties

Figure 6(b) shows a spin-phase plot which results from a spin dynamics run, with the configuration of Fig. 6(a) as the starting configuration. The temperature is $k_BT=0.2J$ and the magnetic field is $h=0.3J$. After just two time steps ($t=0.01/J$) the soliton has disappeared. In Fig. 7 the soliton is still there after a much longer time ($t=15/J$). The temperature in this figure is the same as in Fig. 6 but the field is decreased to $h=0.1J$. From analyzing many more plots like these we find that above a "critical" field the solitons are unstable. We find the stability field

$$h/J=0.2\pm0.1\ . \tag{12}$$

This finding is in good agreement with theoretical calculations.[5,17] In a continuum approximation, an instability field due to out-of-plane fluctuations of the spins is found to be $h=0.4J$.[5] A further calculation taking the discreteness of the lattice into account reduces this prediction to $h=0.2723J$.[17]

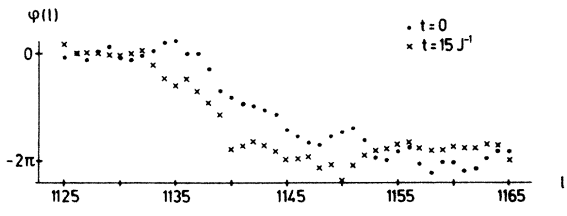

FIG. 7. The figure shows the spin phase ϕ_l as a function of spin site number l. Individual spins can now be resolved. The temperature is the same as in Fig. 7 but the field is reduced to $0.1J$. The soliton is stable and has traveled about four lattice spacings. The field is below the stability field h_s.

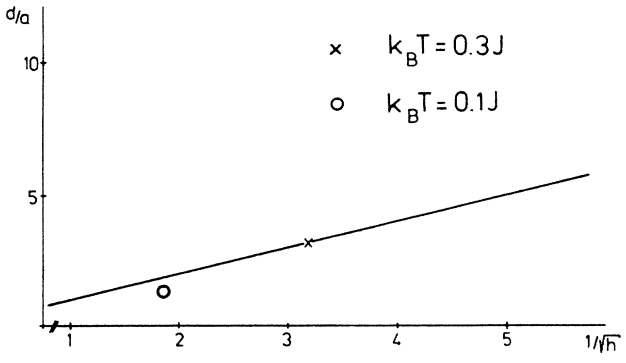

FIG. 8. The field dependence of the width of the solitons. The temperature is as marked. The solid line is the prediction of the sine-Gordon theory.

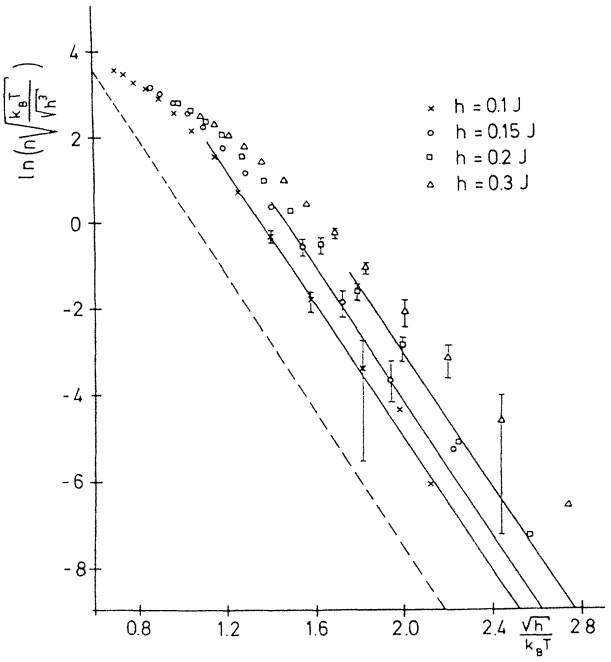

FIG. 9. The soliton density n_k^{tot} in a universal representation. The dashed line indicates the prediction of the sine-Gordon theory [see Eq. (10)]. The solid lines have the same slope as the sine-Gordon prediction.

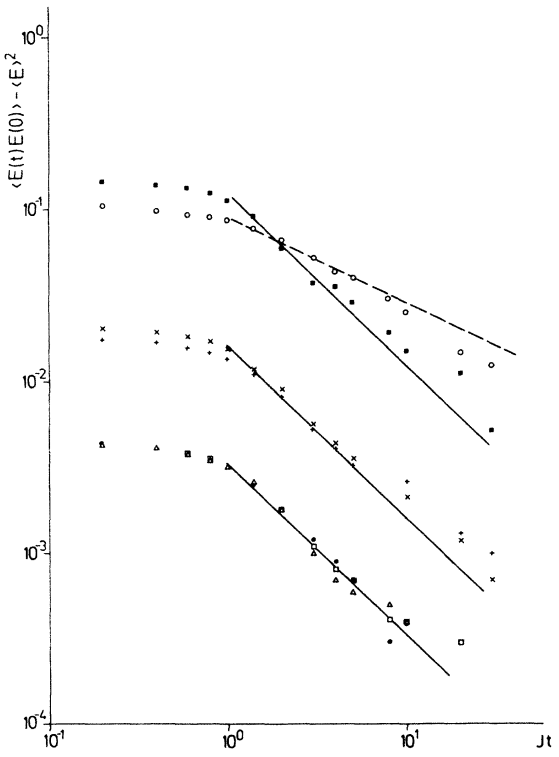

FIG. 10. Time dependence of the energy-energy correlation function for different temperatures and fields. The symbols denote the following. For $k_BT/J=0.1$: ●, $h/J=0.05$; □, $h/J=0.05$; △, $h/J=0.3$. For $k_BT/J=0.2$: +, $h/J=0.1$; ×, $h/J=0.6$. For $k_BT/J=0.5$: ○, $h/J=0.1$; ■, $h/J=1.5$. The solid lines have slope -1 and the dashed line has slope $-\frac{1}{2}$.

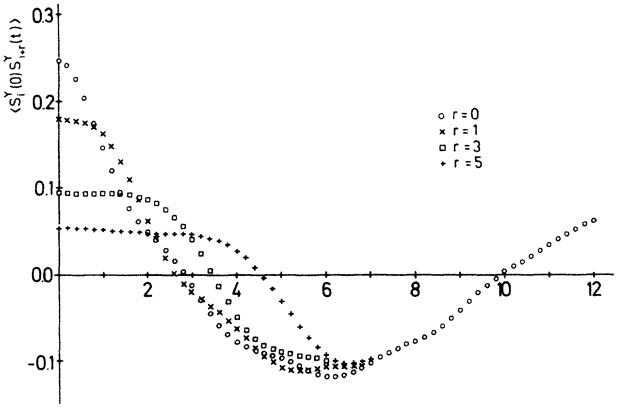

FIG. 11. Time dependence of the y component of the spin-spin correlation function. For clarity, not all data points are plotted. $k_BT/J=0.2$ and $h/J=0.1$.

The time-dependent energy-energy correlation function is plotted in Fig. 10. It is expected that this correlation decays like $t^{-1/2}$.[25] For small fields and large temperature we can observe this behavior, but for large fields it is always a t^{-1} dependence. There is a crossover between these two different decay types as a function of field.

Figure 11 shows the y component of the time-dependent spin-spin correlation function. For short times we see linear spin-wave behavior. This is in agreement with the spin-wave picture by Nelson and Fisher[26] and with our zero-field results.[15] Nelson and Fisher predicted a zero-field behavior, which is given by

$$S_\perp(r,t)=\exp[-1/2\kappa(\,|\,r-ct\,|\,+\,|\,r+ct\,|\,)]\,, \qquad (13)$$

where κ is the inverse correlation length and c is the spin-wave velocity. This correlation function is constant for $t<r/c$ and then decays. For nonzero field the decay is of course not exponential, but nevertheless we see the plateau from Eq. (13). The time for which the correlation function is constant is the time which information needs to travel the distance r and therefore gives a direct measurement of the spin-wave velocity. For long times we

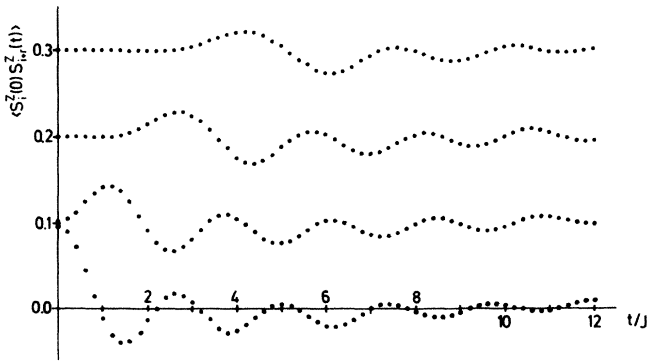

FIG. 12. Time dependence of the z component of the spin-spin correlation function. The position of the first maximum is proportional to the spin-wave velocity. For clarity, the zero line is shifted by 0.1 from curve to curve. $k_BT/J=0.2$ and $h/J=0.1$.

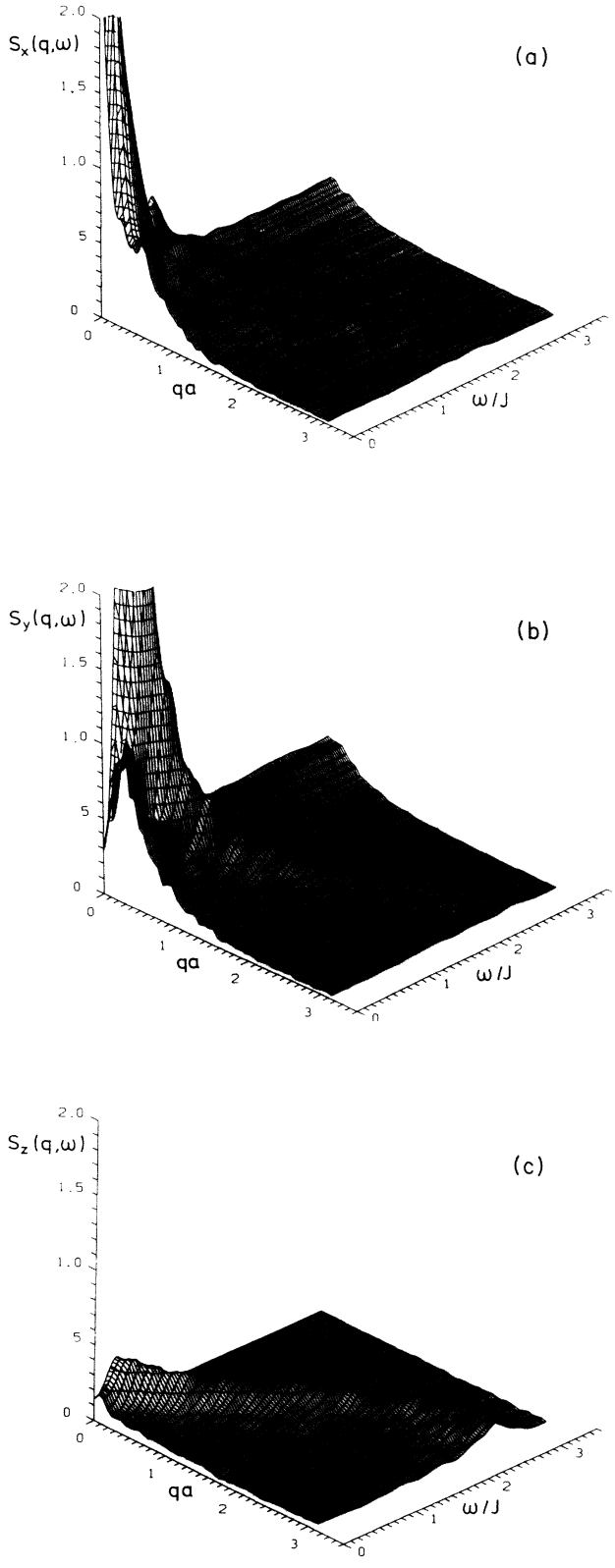

FIG. 13. The components $S_k(q,\omega)$ of the scattering law for $k_BT/J=0.4$ and $h/J=0.1$. The resolution functions described in Eqs. (7) and (8) were used to simulate the finite resolution of a spectrometer. (a) $k=x$, (b) $k=y$, (c) $k=z$. The spatial resolution is in all cases $\Delta q=0.03$ and the energy resolution is $\Delta\omega=0.1J^{-1}$.

see the precession around the magnetic field (large oscillations) and superimposed on it are small oscillations due to spin waves. These small oscillations have the same frequency as the oscillations in Fig. 12. For small fields the z component (Fig. 12) shows pure spin-wave behavior and the position of the first maximum corresponds to the end of the plateau in the y polarization. For large fields the longitudinal spin-spin correlation function exhibits precessional motion around the field.

In Fig. 13 we show the three polarizations of the scattering law $S(q,\omega)$. The fluctuations due to a finite number of configurations and due to the relatively short (compared to macroscopic times) integration times are still noticable.

The scattering function $S_x(q,\omega)$ in Fig. 13(a) shows a large peak at $q=0$ and $\omega=0$. We can see a tiny remnant of the dispersion relation. Nevertheless it does not allow us to extract the dispersion relation. The increase for $q\rightarrow 0$ in the x polarization and in the y polarization stems from errors in subtracting the proper magnetization from the correlation functions. This is the most pronounced influence from the finite number of configurations used in our calculation.

In the scattering functions $S_y(q,\omega)$ and $S_z(q,\omega)$ we can clearly identify the dispersion relation. In Fig. 13(b) a large peak at $q=0$ and $\omega\neq 0$ can also be seen. It decays very fast with increasing q. This peak is broader than the peak in the x polarization. Within the error bars we could not find any differences between the spin-wave dispersion for the two polarizations.

Mikeska[1] predicted a soliton-induced central peak,

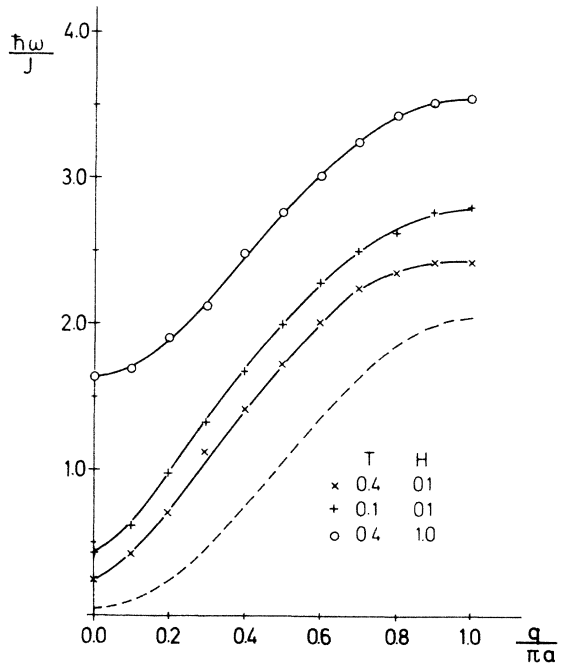

FIG. 14. The spin-wave dispersion curve for different temperatures and fields as determined from the spin-wave peaks in $S(q,\omega)$, e.g., in Figs. 13(a) and 13(b). The solid lines are a guide to the eye only and the dashed lines give the prediction from linear spin-wave theory (harmonic approximation).

which is not obvious in our results. With the quality of the results we have reported here a clear statement concerning this central peak cannot be made. Much larger calculations with much better statistics on configurational averages are necessary to study that peak. We believe that simulations of spin chains with at least $N = 10000$ spins (or at least 25 runs on 2000 spin chains) are necessary to investigate the existence of such a central peak.

From the position of the spin-wave peaks we determined the dispersion curves for different fields and temperatures. In Fig. 14 a typical example for a dispersion curve is shown. It shows the behavior of a linear spin-wave model as qualitatively predicted by a harmonic approximation to the spin Hamiltonian in Eq. (1).[27] The gap indicates the influence of the magnetic field on the spin-wave spectra.

IV. CONCLUSION

Our Monte Carlo results give clear evidence for the existence of spin solitons. They also prove that simple sine-Gordon theory describes some features correctly but fails on others. When the theory is improved, e.g., the discreteness of the lattice is taken into account or the out-of-plane fluctuations are treated, the agreement between theoretical predictions and the Monte Carlo results becomes much better. Nevertheless the missing soliton peak in the specific heat is not understood and further theoretical calculations are needed. In addition to the nonlinear soliton behavior, the system shows clear linear spin-wave behavior even though there is no long-range order. The combination of Monte Carlo and spin dynamics simulations is thus a powerful tool to test analytical approximations and calculations.

ACKNOWLEDGMENTS

One of us (R.W.G.) wishes to thank the Deutsche Forschungsgemeinschaft for support by several travel grants. The work is also supported by the National Science Foundation (NSF) Grant No. DMR-86-03605. The support of Cyber 205 time by the "Advanced Computational Methods Center" at the University of Georgia is acknowledged. We also thank the Institut für Festkörperforschung at the Kernforschungsanlage Jülich for access to the Cray X-MP Computer where parts of the calculations were done.

---

*Permanent address: Institut für Theoretische Physik der Universität Erlangen–Nürnberg, Glückstrasse 6, D-8520 Erlangen, West Germany.

[1]H. J. Mikeska, J. Phys. C **11**, L29 (1978).
[2]J. M. Loveluck, T. Schneider, E. Stoll, and H. R. Jauslin, Phys. Rev. Lett. **45**, 1505 (1980).
[3]H. R. Jauslin, T. Schneider, E. Stoll, and J. M. Loveluck, J. Phys. C **15**, L99 (1982).
[4]T. Schneider, Phys. Rev. B **24**, 5327 (1981).
[5]E. Magyari and H. Thomas, Phys. Rev. B **225**, 531 (1982).
[6]J. K. Kjems and M. Steiner, Phys. Rev. Lett. **41**, 1137 (1978).
[7]M. Steiner, J. Appl. Phys. **50**, 7395 (1979).
[8]T. Goto and Y. Yamaguchi, J. Phys. Soc. Jpn. **50**, 2133 (1981).
[9]A. P. Ramirez and W. P. Wolf, Phys. Rev. Lett. **49**, 227 (1982).
[10]*Magnetic Excitations and Fluctuations,* edited by S. W. Lovesey *et al.* (Springer, Berlin, 1984).
[11]J. F. Currie, J. A. Krumhansl, A. R. Bishop, and S. E. Trullinger, Phys. Rev. B **22**, 477 (1980).
[12]T. Schneider and E. Stoll, Phys. Rev. B **2**, 5317 (1980).
[13]M. G. Pini and A. Rettori, in *Magnetic Excitations and Fluctuations,* Ref. 10.
[14]K. Binder and D. P. Landau, Phys. Rev. B **13**, 1140 (1976).
[15]R. W. Gerling and D. P. Landau, Phys. Rev. B **27**, 1719 (1983).
[16]O. G. Mouritsen, H. Jensen, and H. C. Fogedby, Phys. Rev. B **30**, 498 (1984).
[17]C. Etrich, H. J. Mikeska, E. Magyari, H. Thomas, and R. Weber, Z. Phys. B **62**, 97 (1985).
[18]R. H. Morf and E. P. Stoll, in *Numerical Analysis,* edited by J. Descloux and J. Marti (Birkhauser, Basel, 1977).
[19]T. R. Koehler and P. A. Lee, J. Comput. Phys. **22**, 319 (1976).
[20]G. S. Joyce, Phys. Rev. Lett. **19**, 581 (1967).
[21]N. N. Chen, M. D. Johnson, and M. Fowler, Phys. Rev. Lett. **56**, 904 (1986).
[22]H. J. Mikeska (private communication).
[23]R. W. Gerling and D. P. Landau, J. Magn. Magn. Mater. **45**, 267 (1984).
[24]H. Jensen and H. C. Fogedby (private communication).
[25]D. P. Landau and J. Thomchik, J. Appl. Phys. **50**, 1822 (1979).
[26]D. R. Nelson and D. S. Fisher, Phys. Rev. B **16**, 4945 (1977).
[27]M. Staudinger, thesis, Universität Erlangen–Nürnberg, 1985 (unpublished).

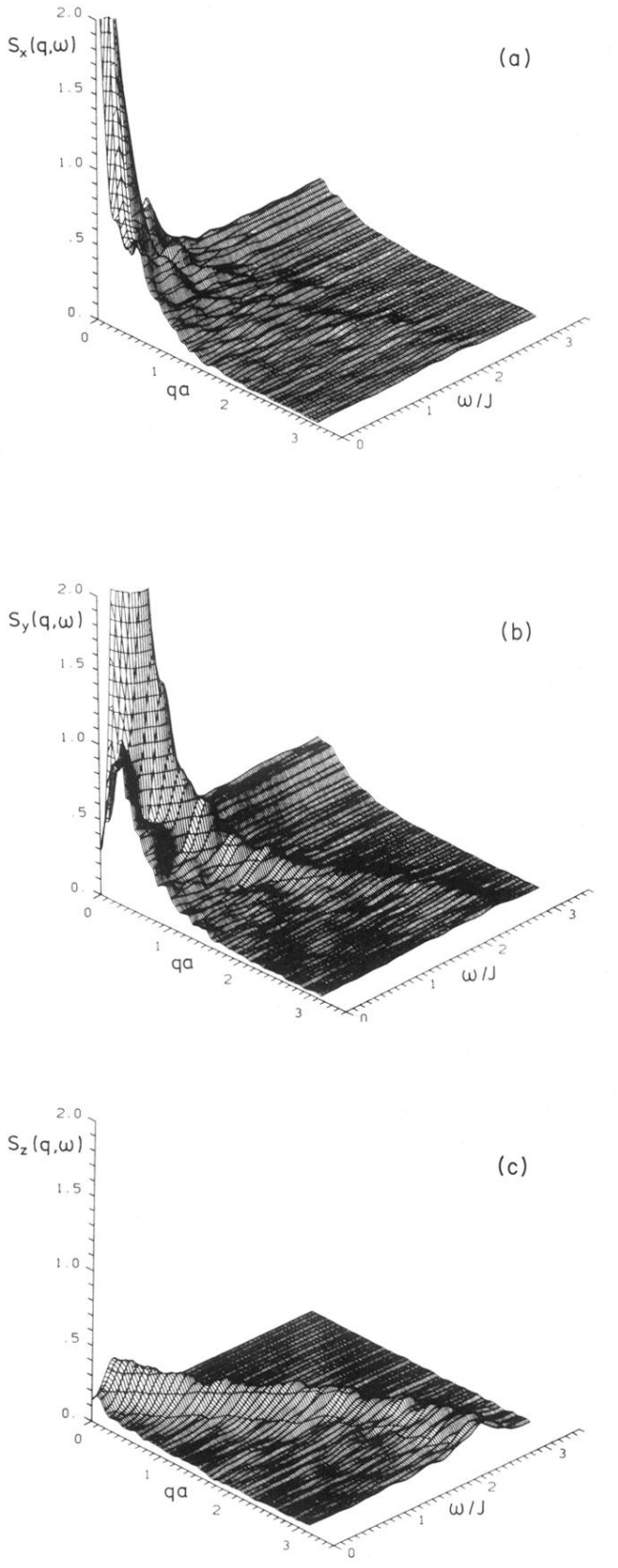

FIG. 13. The components $S_k(q,\omega)$ of the scattering law for $k_B T/J=0.4$ and $h/J=0.1$. The resolution functions described in Eqs. (7) and (8) were used to simulate the finite resolution of a spectrometer. (a) $k=x$, (b) $k=y$, (c) $k=z$. The spatial resolution is in all cases $\Delta q=0.03$ and the energy resolution is $\Delta\omega=0.1J^{-1}$.